The Cryosphere Discuss., 9, 1667–1704, 2015
www.the-cryosphere-discuss.net/9/1667/2015/
doi:10.5194/tcd-9-1667-2015

The Cryosphere Discussions
Open Access

Area, elevation and mass changes of the two southernmost ice caps of the Canadian Arctic Archipelago between 1952 and 2014

C. Papasodoro[1], E. Berthier[2], A. Royer[1], C. Zdanowicz[3,*], and A. Langlois[1]

[1]Centre d'Applications et de Recherches en Télédétection, Université de Sherbrooke, Sherbrooke, Québec, Canada. Centre d'Études Nordiques, Québec, Canada
[2]Laboratoire d'Etudes en Géophysique et Océanographie Spatiales, Centre National de la Recherche Scientifique (LEGOS – CNRS, UMR5566), Université de Toulouse, 31400 Toulouse, France
[3]Department of Earth Sciences, Uppsala University, Sweden
[*]previously at: the Geological Survey of Canada, Northern Division, Ottawa, Canada

Received: 16 February 2015 – Accepted: 2 March 2015 – Published: 16 March 2015

Correspondence to: C. Papasodoro (charles.papasodoro@usherbrooke.ca)

Published by Copernicus Publications on behalf of the European Geosciences Union.

Abstract

In the far south of the Canadian Arctic Archipelago (CAA), on the Meta Incognita Peninsula (Baffin Island, Nunavut, Canada), the small Grinnell and Terra Nivea ice caps have received little attention compared to the much larger ice masses further north. Their evolution can, however, give valuable information about the impact of the recent Arctic warming at lower latitudes (i.e. 62.5° N). In this paper, we measure historical and recent rates of area, elevation and mass changes of both ice caps using in-situ, airborne and spaceborne datasets. Results show that the Terra Nivea Ice Cap (TNIC) areal extent has decreased by 34 % since the late 50s, while the Grinnell Ice Cap (GIC) extent was reduced by 20 % since 1952. For both ice caps, rates of area reduction accelerated at the beginning of the 21st century. The glacier-wide mass balance for the GIC was $-0.37 \pm 0.21\,\mathrm{m\,a^{-1}}$ water equivalent (w.e.) for the 1952–2014 period, and $-0.47 \pm 0.16\,\mathrm{m\,a^{-1}}$ w.e. on the TNIC for the 1958/59–2014 period. More recently, the TNIC has experienced an accelerated rate of mass loss of $-1.68 \pm 0.36\,\mathrm{m\,a^{-1}}$ w.e. between 2007 and 2014. This rate is 5.6 times as negative when compared to the 1958/59–2007 period ($-0.30 \pm 0.19\,\mathrm{m\,a^{-1}}$ w.e.) and 2 times as negative when compared to the mass balance of other glaciers in the southern parts of Baffin Island over the 2003–2009 period. A similar acceleration in mass loss is suspected for the GIC, given the calculated elevation changes and the proximity.

1 Introduction

With a glacierized area of $\sim 150\,000\,\mathrm{km^2}$, the Canadian Arctic Archipelago (CAA) is one of the major glacier regions in the world (Pfeffer et al., 2014). In response to the currently observed warming in the Arctic (Vaughan et al., 2013; Tingley and Huybers, 2013; Kaufman et al., 2009), glaciers have recently experienced an acceleration in their mass loss. For the southern parts of the CAA, annual thinning of glaciers has doubled between the historical (1963–2006) and recent (2003–2011) periods (Gardner et al.,

TCD
9, 1667–1704, 2015

2012). Over the entire CAA, the rate of mass change has tripled between 2004 and 2009, reaching $-92 \pm 12\,\mathrm{Gt\,a^{-1}}$ in 2009 (Gardner et al., 2011), making this region one of the main contributors to eustatic sea-level rise for this period, after Greenland and Antarctica (Gardner et al., 2013; Vaughan et al., 2013). Continued monitoring of CAA glaciers is thus critical.

Located in the southeast part of the CAA, Baffin Island (Nunavut, Canada) is the largest island of the CAA (Andrews et al., 2002) and contains a total ice area of $\sim 37\,000\,\mathrm{km^2}$. In addition to the two major ice caps, Barnes ($\sim 5900\,\mathrm{km^2}$) and Penny ($\sim 6400\,\mathrm{km^2}$), the island is also covered by a number of isolated icefields and small ice caps such as the two southernmost ice caps, Grinnell Ice Cap (GIC) and the Terra Nivea Ice Cap (TNIC) (Fig. 1). Compared to Barnes and Penny ice caps, GIC and TNIC have received little scientific attention so far (Andrews, 2002). Different in situ geophysical measurements were carried out in the 50s (Blake, 1953; Mercer, 1956), and in the 80s by teams from Cambridge University and the University of Colorado (Dowdeswell, 1982, 1984). Other measurements were conducted in the early 90s by a scientific team from Bates College (Maine, USA) and the Nunavut Arctic College. In 2003/04, glaciologists from the Geological Survey of Canada carried out in situ measurements on the GIC (GNSS elevation measurements, automatic weather station installation, snow measurements, stakes, etc.) with the objective to create and maintain a long-term observing site. Consistent prohibitive weather conditions coupled with difficult access to the ice cap have led to the cancellation of the project (Zdanowicz, 2007). An exception is a recent study (Way, 2015) which analyzed the changing rates of areal recession of both GIC and TNIC since the 1950s using historical aerial photographs, satellite (Landsat) imagery and digital elevation models (DEM). In the present study, we supplement these results by presenting a comprehensive analysis of historical and recent fluctuations (1952–2014) of area, surface elevation and mass for the GIC and TNIC over the period 1952–2014. This is done by combining data from spaceborne instruments (e.g., laser altimetry and optical stereo imagery), DEMs, airborne imagery (air photos) and in situ (differential GPS) surveys. Our analysis differs from that of Way (2015) in the

TCD
9, 1667–1704, 2015

choice of photos, DEMs, and spaceborne, remotely-sensed data we used. In particular, we explored the use of sub-meter resolution stereo pairs obtained from the new Pléiades satellites to derive accurate DEMs and to collect accurate, numerous and homogeneously distributed ground control points (GCPs) for the photogrammetric processing of aerial photos archives. We place our findings in the context of the observed pattern of regional glacier changes across the CAA, and discuss possible climatic forcing factors of particular relevance for the southernmost Baffin Island region.

2 Study area

The GIC and TNIC (Fig. 1) are located on the Meta Incognita Peninsula, 200 km south of Iqaluit, Nunavut. The GIC (62.56° N, 66.79° W) covers an area of 107 km^2 (August 2014; this study) with the highest elevations rising at 800 m above sea level (a.s.l.). On the northeast side, some outlet glaciers extend near Frobisher Bay, which connects to the ocean. The TNIC (62.27° N, 66.51° W) is located ~ 17 km south of the GIC. It covers an area of approximately 150 km^2 (August 2014; this study) with a similar elevation range to the GIC. Mercer (1954) suggested three factors supporting the continued presence of plateau ice caps on Meta Incognita Peninsula: (1) cool summers (2) frequent low-level cloudiness and (3) heavy snowfall. Data from the weather station in Iqaluit (34 m a.s.l. and ~ 200 km northwest of the two ice caps) indicate that winter temperatures in this region averaged −24 °C over the past 60 years, while mean summer temperatures ranged between 6 and 7 °C. Total annual precipitations reached ~ 500 mm (snow: ~ 300 mm; rain: ~ 200 mm). For both the GIC and TNIC, any present-day accumulation is likely only in the form of superimposed ice, i.e. ice formed by in situ refreezing of snow meltwater. Field observations in winter 2003/04 showed no firn at the summit of GIC, and the estimated net winter snow accumulation there (~ 2–3 m snow; or ~ 0.65–0.75 m water equivalent) was approximately equal to the rate of surface lowering by melt in summer (Zdanowicz, 2007). Hence the summit of the GIC is probably very close, or slightly below, the present-day equilibrium line altitude (ELA).

TCD
9, 1667–1704, 2015

Observations from various expeditions in the 50s revealed that the western margin of the GIC was relatively stable, but that outlet glaciers were shrinking moderately when compared to photographs from 1897 (Mercer, 1954, 1956). Moraines studied near both ice caps in the early 80s indicated that the main retreat dated from the last 100 years and that both ice caps were probably at their largest areal extent during the Little Ice Age cold climate interval (Muller, 1980; Dowdeswell, 1982, 1984; Andrews, 2002). Dowdeswell (1982) estimated that the outlet glacier of the GIC that calves into Watts Bay extended much further out a few centuries earlier, but also reported that another outlet glacier to the south of the ice cap was advancing.

3 Data

3.1 Pléiades stereoscopic images

Launched respectively on 17 December 2011 and 2 December 2012, the Pléiades 1A and 1B satellites have recently shown their high potential for DEM extraction on glaciers and thus, for mass balance calculations (Wagnon et al., 2013; Berthier et al., 2014). The two satellites follow the same near-polar sun-synchronous orbit and provide panchromatic and multispectral imagery at a very high ground spatial resolution, i.e. 0.7 m for panchromatic and 2.8 m for multispectral images (Astrium, 2012). Both satellites have independent stereoscopic capabilities. The fact that the panchromatic band images derived from Pléiades satellites are coded in 12 bits represents a clear advantage on a glacier surface (especially accumulation area), given the fact that a large radiometric range provides better contrast and limit the risk of image saturation (Berthier et al., 2014).

Three stereoscopic pairs were acquired over our study area (Table 1): one for the GIC (3 August 2014) and two for the TNIC (14 August 2014 for the eastern part and 26 August 2014 for the western part). The stereoscopic pair covering the GIC is cloud-free while a few clouds (< 10 %) were present during the two TNIC acquisitions (Fig. 2).

TCD
9, 1667–1704, 2015

Acquisitions were made at the end of the ablation season to ensure a maximum degree of texture due to a more humid surface (Berthier and Toutin, 2008). This is particularly true for the present images, since the ice caps were nearly winter snow free. Thereby, this is a good qualitative primary concern about the ice caps' fate (Pelto, 2010). Each image was provided with Rational Polynomial Coefficients (RPCs), which allows geometric modeling without GCP. Those stereoscopic pairs were used (1) for the generation of recent DEMs on both ice caps and (2) for GCP extraction for the photogrammetric processing of the historical aerial photos on the GIC.

3.2 Historical aerial photos

Archives aerial photos covering the GIC were obtained through the *Canadian National Air Photo Library* (Natural Resources Canada archives). In this study, we used 24 photos acquired at the end of the ablation season, on 21 and 22 August 1952. A Williamson Eagle IX Cone 524 camera type with a focal length of 152.15 mm was used and the flight altitude was 16 000 ft (4879 m). The photos are distributed in 3 parallel flight lines with an overlapping coverage of ~ 30 % between each line and ~ 60 % between two photos of a same line. On these images, the surface texture of the GIC is clearly visible, mainly due to the late summer acquisition date. These photos, exceptional in their quality of detail compared to later series (1958 onwards) taken from higher altitudes, were used for the extraction of historical elevations on the GIC and were thus preferred to the Canadian Digital Elevation Data (CDED), given numerous artefacts contained in the latter, especially in the accumulation area.

3.3 Historic Canadian Digital Elevation Data (CDED)

Historic CDED provided at a scale of 1 : 50k (Natural Resources Canada) were acquired for the two ice caps. These elevations were created by stereo-compilation of aerial photos acquired during summers 1958 and 1959. Raw elevations are orthometric and referenced to the Canadian Gravitational Vertical Model of 1928 (CGVD1928).

TCD
9, 1667–1704, 2015

The average elevation differences and their standard deviation (SD) were previously calculated off glacier between 21 Arctic CDED maps tiles and ICESat laser altimetry points and were reported to be 0.3 and 6.2 m, respectively (Beaulieu and Clavet, 2009). Here, CDED were used (1) as historical elevations for the TNIC and (2) the surrounding ice-free elevations were used for the absolute coregistration for both ice caps (see Sect. 4.3). Artefacts located in the accumulation areas of the TNIC CDED were manually deleted using the derived hillshade in order to exclude obviously false elevations. Those artefacts were less pronounced than for the GIC CDED and were likely due to the poor contrast and low texture of the 1958/59 aerial photos that were used to generate the CDED.

3.4 ASTER DEM

Products derived from the ASTER satellite mission have been widely used for glaciological studies (e.g., Frey et al., 2012; Nuth and Kääb, 2011; Das et al., 2014). In order to calculate a recent mass balance rate for the TNIC, we used a DEM (product AST14DMO) generated from an ASTER stereo pair acquired on 3 August 2007. This DEM was automatically derived from bands 3N (nadir-viewing) and 3B (backward-viewing) that have an intersection angle of 27.6°, which corresponds to a base-to-height ratio of 0.6 (Fujisada et al., 2005). The raw DEM was provided with an horizontal grid spacing of 30 m and elevations are orthometric to the EGM96 geoid. Using 57 ICESat points from two different time periods, namely a few months before (April 2007) and after (November 2007) the ASTER acquisition, we assessed a vertical precision of 2.5 m (SD) on the ice cap for this ASTER DEM. Due to cloud coverage, no ASTER DEM was available for the GIC at the end of the ablation season.

3.5 ICESat altimetric points

Surface elevation profiles (GLA14, Release 634) collected by the Geoscience Laser Altimetry System (GLAS) onboard ICESat were acquired (Zwally et al., 2002). Each laser

TCD
9, 1667–1704, 2015

pulse-derived corresponds to field-of-view with a diameter of ~ 65 m and a spacing of 172 m between each footprint (Schutz et al., 2005). ICESat elevations were converted from their original Topex Poseidon ellipsoid to the WGS84 ellipsoid using tools provided by the National Snow and Ice Data Center. The entire dataset (2003 to 2009) was used for absolute coregistration on ice-free terrain, while the data collected during a few selected dates (Table 1) were used for recent elevation change calculations over the ice caps.

3.6 In-situ GPS measurements

In April 2004, a team from the Geological Survey of Canada measured three surface elevation profiles at 50 m horizontal intervals using a Trimble® high-precision Real-Time Kinematic (RTK) GPS system on the southeast, west and northwest sides of the GIC, and at the front of an outlet glacier (Zdanowicz, 2007). Data acquisition was made using a fixed base station on a geodetic benchmark monument, and GPS positions were subsequently processed with the Canadian Center for Remote Sensing's Precise Positioning System (PPS) to obtain an accuracy of a few cm. For this paper, those transects were used for recent elevation change calculations. It is known that elevations calculated using Precise Positioning System and referenced to the GRS80 ellipsoid can be assumed equal to the WGS84 ellipsoid (sub-mm differences).

3.7 Glacier outlines

Various datasets have been used to extract the areal extent of the two ice caps at the end of the ablation season (August–September). For the GIC, three datasets from different dates were used. The 1952 outline was derived manually from the orthorectified historical aerial photos. The Randolph Glacier Inventory (RGI 3.2; Pfeffer et al., 2014) ice cap contour was used for 1999, while we manually digitized the 2014 margin from the orthorectified panchromatic Pléiades image. For the TNIC, outlines were derived for four different dates. We used the raw vectors from the 1 : 250k Canadian National

TCD
9, 1667–1704, 2015

Topographic Data Base as the 1958/59 boundary. Given the anomalies perceived in the interpretation of the 1999 margin from the RGI 3.2 (i.e. snow covered terrain included in the glacier extent), we rather manually digitized the ice cap margin using a 30 m resolution Landsat 5 image acquired on August 1998. The August 2007 limit was manually traced from an ASTER orthoimage (15 m of resolution) provided with the on-demand AST14DMO product, while the 2014 margin was extracted from the orthorectified panchromatic Pléiades images (East and West). To decrease the effect of cloudiness on the Pléiades orthoimages (~ 20 % of the ice cap outline), we used a Landsat 8 panchromatic (15 m of resolution) image also acquired in August 2014. The uncertainty assessment of the outlines is briefly presented in Sect. 4.4.3.

3.8 Meteorological and sea ice records

In order to quantify changes in the regional climate of southern Baffin Island region over the period covered in our study, air temperature records were retrieved from the Iqaluit weather station for 1950–2014 (http://climat.meteo.gc.ca/). This is the station in the eastern Canadian Arctic with the most continuous records extending back more than a few decades. Furthermore, sea ice covered area of the Hudson Strait and Davis Strait were obtained from the Canadian Ice Service archives for the 1968–2014 period (http://www.ec.gc.ca/glaces-ice/).

4 Methods

4.1 Pléiades DEM generation

The Pléiades DEMs were generated using the OrthoEngine module of Geomatica 2013. No GCP were available for the geometric correction so we relied on the RPCs provided with the images. Adding GCP does not improve the vertical precision of the Pléiades DEM, but only allows reducing the vertical bias (Berthier et al., 2014). The

TCD
9, 1667–1704, 2015

latter bias can be easily corrected on ice-free terrain with a good reference dataset, such as ICESat.

The following steps of DEM extraction were repeated for the 3 Pléiades stereoscopic pairs. First, we collected 20 tie points (TPs) outside and 6 on the ice cap. Collecting well-distributed TPs was found to improve the relative orientation between the two images providing increased coverage (Berthier et al., 2014). For the DEM extraction, the following processing parameters were used in OrthoEngine: the relief type was set to *Mountainous* and the DEM detail to *Low*. No interpolation was performed to fill data gaps so that the resulting DEMs do not contain interpolated elevations. Finally, the DEMs were geocoded with a pixel size of 4 m.

Since the ice-free zones on our Pléiades DEM were not large enough to calculate an elevation accuracy with a sufficient number of ICESat points, we report here the vertical precisions obtained in recent glaciological studies. For example, Wagnon et al. (2013) measured an accuracy of 1 m (SD) on a glacier surface in Himalaya using Pléiades DEM. Berthier et al. (2014) also obtained an accuracy ranging between 0.5 and 1 m (SD), highlighting the precision consistency on glacier surfaces. This accuracy was shown to be mostly correlated with slope. A similar vertical precision is thus expected here.

4.2 Aerial photos DEM generation

Photogrammetry is an effective technic for glaciology studies, particularly used for terrain reconstruction prior to the modern satellite era (Fox et Nuttall, 1997; Barrand et al., 2009). A 1952 DEM of the GIC was created using OrthoEngine. This software uses a mathematical model compensating for both terrain variation and inherent camera distortions (PCI Geomatics, 2013). The typical photogrammetric procedure was then followed to compute the model and thereby solving the least-square bundle adjustment.

Collecting effective GCPs for photogrammetry purposes in mountainous or polar regions remains one of the main difficulties, especially for archive photos (Barrand et al., 2009). To overcome this difficulty, Pléiades derived products (DEM and orthoimage)

TCD
9, 1667–1704, 2015

were used to collect GCPs. For each aerial stereoscopic model partially covering the surrounding ice-free terrain, 3 to 7 GCPs were collected outside the ice cap on topographic or geomorphologic structures visible on both the Pléiades orthoimage and the aerial photographs. In order to strengthen the mathematical model, every GCP was collected as stereo GCP, i.e. was identified in all possible aerial photographs. A total of 39 stereo GCPs were collected resulting in 106 GCPs. Also, 6 to 10 TPs per aerial stereoscopic model were collected dispersedly. For the models situated in the middle of the photogrammetric block and covering only the ice cap (no stable terrain), only TPs were collected in order to connect them to the photogrammetric block. After the final bundle adjustment, the resulting residual averages of all the GCPs were 2.85 m in X, 2.74 m in Y and 2.68 m in Z. TPs residuals were 1.84 m in X and 2.15 m in Y. The generated global DEM was geocoded with a grid resolution of 10 m and no interpolation of data gaps was performed.

Validation of the resulting DEM (before coregistration) against 76 ICESat points on ice-free terrain showed a mean offset of −3.29 m (ICESat below in elevations) and a SD of 4.96 m. Moreover, the SD of the elevation differences measured outside the ice cap between the Pléiades DEM and the 1952 DEM (coregistered together, see Sect. 4.3) was 13.8 m, while 16.5 m was measured on the ice cap. Quantitatively, 66 % of the GIC area was extracted with data gaps concentrated at the highest elevation in the texture-less accumulation areas.

4.3 DEM adjustments and coregistrations

DEM coregistration is of primary importance before performing any DEM-based mass balance calculation (Nuth and Kääb, 2011). This 3-D coregistration method uses the relation between aspect, slope and elevation differences over ice-free terrain (Nuth and Kääb, 2011) using ICESat as reference. The Pléiades images only included a small corridor (~ 20 km^2) of ice-free terrain near the ice caps (Fig. 2). This corridor coincides with limited number of cloud-free ICESat shots (less than 100 for each ice cap) so that a direct coregistration between the Pléiades DEM and ICESat was not possible. Instead,

TCD
9, 1667–1704, 2015

the CDED tile encompassing the two ice caps was first coregistered with approximately ~ 1000 ICESat points over ice-free zones. All other DEMs were then 3-D coregistered to the corrected CDED, independently for each ice cap and the corrected datasets were referenced to the WGS84 ellipsoid. To evaluate the corrections consistency, the offset over ice-free terrain between each corrected DEMs and corresponding ICESat points were verified. However, one must interpret these results carefully given the sparsely distributed and limited number of ICESat points (less than 100) over moderate to hilly terrain. The offset was below 1.5 m in each case, suggesting that the absolute coregistration was well conducted and that the effect of geoid variations (CGVD1928 and EGM96 vs. WGS84) was negligible for such small zones.

Furthermore, the two independently coregistered Pléiades DEM of the TNIC (14 and 26 August) were subtracted in order to analyze the overlapping zone (Fig. 2). The corresponding offset measured over the ice-free terrain was −0.1 m, while an average elevation difference of about 0.64 m was measured over the ice cap, probably due to the thinning between 14 and 26 August. These results prove the robustness of the 3-D coregistration using the corrected CDED DEM.

4.4 Elevation changes and mass balance calculation

4.4.1 Elevation changes along ICESat and GPS tracks

For both ice caps, recent elevation changes were measured between 6 ICESat tracks, from different laser overpass periods (autumn 2003 to winter 2007), and the 2014 Pléiades DEMs. For the GIC only, elevation changes were also calculated between the April 2004 in situ GPS transects and the 2014 Pléiades DEM. We did not attempt to compute a glacier-wide mass balance from those recent elevation changes measurements since (i) they are sparse and only cover a small fraction of the two ice caps and (ii) GPS and some of the ICESat data were acquired at the end of winter and limited data were available to apply a seasonal correction. Nevertheless, those recent

TCD
9, 1667–1704, 2015

elevation changes along selected tracks are useful to complement the differential DEM analysis described below.

4.4.2 DEM derived elevation changes and mass balances

The geodetic method was applied using the different DEMs in order to calculate glacier-wide elevation changes and mass balances. The following steps were performed for each calculation.

The coregistered DEMs were first subtracted in order to obtain maps of elevation changes (dH), or elevation change rates (dH/dt) after dividing by the interval time. dH were binned into 50 m elevation bands and averaged after applying a three sigma filter to exclude outliers (Gardner et al., 2012; Gardelle et al., 2013). The *no value* pixels were assigned to the mean dH of the corresponding elevation band. Total volume change for an ice cap (dV) was then assessed by summing volume changes from all elevation bands (n) as follows:

$$\mathrm{d}V = \sum_{i}^{n} (\Delta H_i \cdot A_i), \quad (1)$$

where i corresponds to an elevation band of 50 m, ΔH is the mean elevation change measured at elevation band i and A_i is the area of the elevation band. Hypsometry is based on the 1 : 250k CDED (1958/59) while the ice cap limit is conform to the year of the oldest DEM used in the calculation. Sensibility tests have shown that the choice of the DEM used to derive the hypsometric analysis has a very low impact on the mass balance calculation ($< 0.01\,\mathrm{m\,a^{-1}}$ w.e.) as also demonstrated in Gardner et al. (2011).

The elevation change rate averaged over the entire ice cap (glacier-wide), $\mathrm{d}H/\mathrm{d}t_{\mathrm{avg}}$, was then calculated as follows:

$$\mathrm{d}H/\mathrm{d}t_{\mathrm{avg}} = \frac{\mathrm{d}V}{(\overline{A} \cdot \Delta t)}, \quad (2)$$

TCD
9, 1667–1704, 2015

where $\overline{A}$ is the average between initial and final ice cap areas and Δt is the time interval between the two DEMs. In the following sections, dH/dt (raw elevation change rate resulting from coregistered DEM subtraction) was distinguished from dH/dt_{avg}.

Finally, the area-averaged specific geodetic mass balance rate ($m\,a^{-1}$ w.e.), dM/dt, was calculated as follows:

$$dM/dt = dH/dt_{avg} \cdot \rho \quad (3)$$

where ρ is the density constant of $850\,kg\,m^{-3}$ (Huss, 2013). For the sake of readability, the area-averaged specific geodetic mass balance rate (Cogley et al., 2011) is hereafter simply referred as mass balance or glacier-wide mass balance.

4.4.3 Accuracy assessment

The main sources of uncertainty in our mass balance retrieval are related to uncertainties in the elevation change measurements, the ice cap limits and the density used to convert volume to mass changes. For historical measurements, elevation change uncertainty was assumed equal to the SD over stable terrain between the two coregistered DEMs (GIC 1952–2014: 13.8 m; TNIC 1958–2007: 9.6 m; TNIC 1958–2014: 9 m), assuming that elevation errors were 100 % correlated. This is a conservative approach that takes into account both the highly correlated CDED elevation errors (Gardner et al., 2012) and the possible errors associated to the aerial photos-derived DEM (i.e. artefacts and low coverage at higher altitudes).

On the other hand, spatial autocorrelation between the ASTER 2007 and Pléiades 2014 DEMs was analyzed on ice-free terrain to better characterize the elevation change uncertainty in the recent mass balance estimation on the TNIC. A low autocorrelation distance (< 100 m) was found between the two elevation products. Applying standard principles of error propagation (e.g., Zemp et al., 2013), we found a very low (±0.1 m) and probably underestimated uncertainty for the elevation change averaged over the entire ice cap. Consequently, it was instead conservatively assumed that the

TCD
9, 1667–1704, 2015

uncertainty for the elevation changes was equal to the quadratic sum of the two DEMs uncertainties (±1 m for the Pléiades DEM and ±2.5 m for the ASTER DEM), assuming that (i) the elevation errors are fully correlated within each DEM and that (ii) errors of the two DEMs are independent.

We estimated an error of 3 % for the ice caps outlines. This represents a synthesis of both the areas of possible image interpretation errors (< 2 % of each ice cap extent) and the impact of the image resolution used for outlines delimitation (< 1 % of each ice cap extent). Since the ice caps were not covered by debris, interpretation errors were mainly related to the snow-covered surfaces (i.e. snow patches) around each ice cap. The error attributed to the image resolution was established from a comparison analysis made between the Pléiades and Landsat 8 derived outlines, for which a small difference in extent was obtained (< 1 %). The total uncertainty of 3 % was used for mass balance estimation as well as for area change analysis. This uncertainty is comparable to results presented in Paul et al. (2013) and Winsvold et al. (2014). Finally, an uncertainty of $\pm 60\,\mathrm{kg\,m^{-3}}$ was assigned to the density factor when converting from volume change to mass change (Huss, 2013).

5 Results

5.1 Area changes

Areal changes measured for Grinnell and Terra Nivea ice caps since the 50s are shown in Fig. 2. The GIC has experienced a rate of area change of -0.10 ± 0.003 (± 3 %) $\mathrm{km^2\,a^{-1}}$ between 1952 and 1999, whereas a rate of $-0.59 \pm 0.02\,\mathrm{km^2\,a^{-1}}$ is measured for the TNIC between 1958/59 and 1998. These rates of area change have been significantly more negative since 1998/99 reaching $-1.69 \pm 0.05\,\mathrm{km^2\,a^{-1}}$ for the TNIC and $-1.37 \pm 0.04\,\mathrm{km^2\,a^{-1}}$ for the GIC. For the GIC, the 2014 areal extent is about 20 % smaller than during the 50s, while the TNIC area has shrunk by 34 % between 1958/59 and 2014.

TCD
9, 1667–1704, 2015

5.2 Elevation changes

Maps of historical and recent elevation change rates (dH/dt) for the two ice caps are presented in Figs. 3–5 and trends of dH/dt as a function of elevation are shown in Figs. 4–6.

The historical (1952–2014) glacier-wide averaged elevation change rate (dH/dt_{avg}) for the GIC was measured at $-0.44 \pm 0.25\,m\,a^{-1}$, a less pronounced rate when compared to TNIC that experienced a rate of $-0.56 \pm 0.19\,m\,a^{-1}$. Similar patterns of historical dH/dt are observed for both ice caps (Fig. 6 and dH/dt maps), revealing an average surface lowering reaching $-1.1 \pm 0.25\,m\,a^{-1}$ for the GIC and $-0.9 \pm 0.19\,m\,a^{-1}$ for the TNIC in the lower altitudes (i.e. the outlet glaciers in the peripheries). For elevations above 250 m a.s.l., the thinning rate is consistently more negative for the TNIC, compared to the GIC, at an average of $-0.1\,m\,a^{-1}$. On the GIC, the surface thinning was similar for all outlet glaciers between 1952 and 2014 (Fig. 3) while for the TNIC, a stronger lowering ($< -1\,m\,a^{-1}$) was experienced on the northeast outlet glaciers between 1958/59–2007 (Fig. 5, upper left map).

Elevation change rates sharply decreased in the recent years for both ice caps. On the TNIC, the recent (2007–2014) dH/dt_{avg} was $-1.97 \pm 0.40\,m\,a^{-1}$, a rate 5.6 times as negative than the rate of $-0.35 \pm 0.22\,m\,a^{-1}$ measured between 1958/59 and 2007. The acceleration of the thinning rate is particularly strong at lowermost altitudes ($-6.7 \pm 0.40\,m\,a^{-1}$ between 2007 and 2014 vs. $-0.9 \pm 0.22\,m\,a^{-1}$ between 1958/59 and 2007), but is also unambiguously observed in the upper sections of the accumulation area ($-1.7 \pm 0.40\,m\,a^{-1}$ between 2007 and 2014 vs. $-0.3 \pm 0.22\,m\,a^{-1}$ between 1958/59 and 2007).

On the GIC, a comparison of recent and historical dH/dt was conducted over the merged in situ GPS points and ICESat transects from March–April 2004 (Fig. 4). This is the only recent period with a reasonable coverage of the whole ice cap although restricted to 4 transects. One should note that given the limited information available about the seasonal height fluctuation, no correction was applied to account for the

TCD
9, 1667–1704, 2015

different elevation acquisition periods of 1952 and 2014 (August) and 2004 (March–April). For the 203 points where elevation measurements are available in 1952, 2004 and 2014 (points superposed with black dots on the Fig. 4), the recent dH/dt was up to 6 times more negative for the 2004–2014 period ($-1.47\,\mathrm{m\,a^{-1}}$) when compared to the 1952–2004 period ($-0.25\,\mathrm{m\,a^{-1}}$).

Additionally, the elevation changes measured between ICESat same-track transects and Pléiades DEM are shown in Fig. 7. This analysis reveals (1) a very similar variability of annual elevation changes between both ice caps during the 2003–2007 interval and (2) heterogeneous but coherent seasonal fluctuations (March > November). The absolute difference in elevation change between 2003 and 2014 for the two ice caps (total thinning of ~ 11 m for the GIC and of ~ 16 m for the TNIC) is likely at least partly explained by the fact that ICESat transects covering the GIC are located at higher altitudes (~ 65 m in average) than the transects on the TNIC.

5.3 Mass balances

Mass balances for both ice caps are summarized in Table 2. Between 1952 and 2014, a mass balance of $-0.37 \pm 0.21\,\mathrm{m\,a^{-1}}$ w.e. was measured on the GIC. The historical mass balance for the TNIC (1958/59–2014) was more negative at $-0.47 \pm 0.16\,\mathrm{m\,a^{-1}}$ w.e. This long-term average encompasses two different periods with a mass loss 5.6 times greater for the period 2007–2014 (mass balance: $-1.68 \pm 0.36\,\mathrm{m\,a^{-1}}$) when compared to the period 1958/59–2007 (mass balance: $-0.30 \pm 0.19\,\mathrm{m\,a^{-1}}$). As previously discussed (Sect. 5.2), the GIC has likely experienced a similar acceleration of its mass loss since, 2004. However, no reliable recent mass balance could be estimated given the lack of comprehensive coverage (i.e. either altimetry data or DEM) in the 2000s for this ice cap.

TCD
9, 1667–1704, 2015

6 Discussion

6.1 Pléiades as a tool for photogrammetric GCPs collection

In many regions of the world, vast archives of historical aerial photographs represent a potential gold mine for glaciologists in order to depict the multi-decadal volumetric change of glaciers and ice caps (e.g., Soruco et al., 2009; Zemp et al., 2010). The DEM generated from these aerial photographs allows comparing historical and recent mass losses in order to put in a longer-term perspective the recent glacier mass variations. However, these data remain difficult to exploit due to the logistical difficulties involved in the field collection of accurate and well-distributed GCPs in the remote high latitude or high altitude regions. Field GCPs were lacking for the two ice caps studied here, however, we took advantage of the very high resolution of the Pléiades imagery (0.7 m) and the vertical precision of the derived DEM (< 1 m) in order to collect a sufficient number of GCPs for the adjustment of the stereo-model. GCPs were collected on well-defined features that were clearly identifiable on both the Pléiades imagery and the old aerial photos. GCP residuals of ∼ 2–3 m in average were obtained after the block bundle adjustment, and a DEM precision of ∼ 5 m (1-sigma confidence level) was measured with a few ICESat points available over ice-free terrain. This is a satisfactory result given that the aerial photos used here were affected by film distortions that could not be corrected. Our results demonstrate the efficiency of using Pléiades stereo-images to collect accurate GCPs for photogrammetric processing of old aerial photographs in remote environments.

6.2 Comparison to other studies

Our estimates of shrinkage for the GIC and TNIC can be compared with other studies from Baffin Island to verify the coherence of results and get a more complete picture of the pattern of glacier changes across this vast region.

TCD
9, 1667–1704, 2015

Sharp et al. (2014) reported rates of areal change for the TNIC between 1958 and 2000 of up to $-0.66\,km^2\,a^{-1}$ (197 to $169\,km^2$), while our own results give a nearly identical figure of $-0.59 \pm 0.02\,km^2\,a^{-1}$ (196.2 ± 9.9 to $173.2 \pm 8.5\,km^2$) over this similar period. For the GIC, however, the shrinkage rate of $-0.36\,km^2\,a^{-1}$ (135 to $120\,km^2$) reported by Sharp et al. (2014) over the period 1958–2000 is three to four times as negative as our own figure of $-0.10 \pm 0.003\,km^2\,a^{-1}$ for 1952–1999 (131.8 ± 6.6 to $126.9 \pm 6.3\,km^2$). Way (2015) recently reported that between 1973 and 2013, the TNIC area decreased by 22 % (199.1 to $154.8 \pm 7.5\,km^2$), while the GIC areal extent reduced by 18 % (134.3 to $110 \pm 0.9\,km^2$). Results of Way (2015) are superposed in Fig. 8 (lower panel). Hence, even though the results are slightly different between the three studies, our results agree within the error bars when given. We hypothesize that those small disparities could be explained by the interpretation of snow patches around the ice caps, as well as by the different spatial resolutions and acquisition dates of the data source (Paul et al., 2013).

Gardner et al. (2012) estimated that the average mass loss rate of all glaciers and ice caps on southern Baffin Island (South of 68.6° N, excluding the Penny Ice Cap) increased by almost 4 times (i.e. -0.20 ± 0.05 to $-0.76 \pm 0.12\,m\,a^{-1}$ w.e) between the periods 1957–2006 and 2003–2009. This acceleration is more than twice that estimated over similar periods for northern Baffin Island glaciers (North of 68.6° N, excluding the Barnes Ice Cap). The Barnes Ice Cap itself, located on central Baffin Island at elevations between 400 and 1100 m a.s.l., recently experienced a strong thinning acceleration (Sneed et al., 2008; Dupont et al., 2012), resulting in a mass loss rate of $-1.08 \pm 0.12\,m\,a^{-1}$ w.e between 2005 and 2011 (Gardner et al., 2012). The estimated mass loss rates on Penny Ice Cap between 2003 and 2009 is lower at $-0.52 \pm 0.12\,m\,a^{-1}$ w.e., a difference which Gardner et al. (2012) attribute to the higher elevation range (up to ~ 2000 m a.s.l.) of the Penny Ice Cap. The comparatively larger mass loss rates experienced by the GIC and TNIC in the past half-century can be ascribed to differences in size and to the hypsometry of the ice caps, but also possibly to local climatic factors, as described below.

TCD
9, 1667–1704, 2015

6.3 Regional context and climatic factors

The accelerating recession of glaciers and ice caps across the CAA in recent decades has been ascribed to warming Surface Atmospheric Temperatures (SAT) during this period, a situation that results from a sustained atmospheric circulation pattern in the eastern Arctic that enhances advection of warm air from the northwest Atlantic (Sharp et al., 2011). This situation has led to warmer, longer summer melt periods on glaciers of the eastern CAA, and this largely accounts for their increasingly negative mass balance (Weaver, 1975; Hooke et al., 1987; Koerner, 2005; Sneed et al., 2008; Gardner et al., 2012).

On southern Baffin Island, the > 50 year long SAT record from Iqaluit shows that summer temperatures increased by 0.72 °C between 1958–2007 (mean: −0.14 °C) and 2007–2014 (mean: 0.58 °C), relatively to the 1950–2014 mean. Climate records from stations further south (ex: Resolution Island, 61.5° N) are unfortunately too discontinuous to allow quantification of SAT changes on Meta Incognita Peninsula, but these are probably close to those observed in Iqaluit. Although the GIC and TNIC are only separated by 17 km, they did not experience the same historical rates of shrinkage and mass loss (Figs. 3–5), and part of the difference is likely due to differences in hypsometry, which strongly influences the response of glaciers to a given climate forcing (Oerlemans et al., 1998; Davies et al., 2012; Hannesdottir et al., 2014). The GIC lies at slightly higher altitude than the TNIC, with 77 % of its area above 600 m a.s.l., compared to 68 % for the TNIC, and is therefore expected to have a slightly less negative mass balance, as our observations confirm.

An important factor that likely contributed to the accelerating rate of glacier recession on southernmost Baffin Island is the decline in summer sea ice cover in this region (Fig. 8b and c), one of the steepest observed across the entire CAA (up to −16 % decade^{-1} since 1968; Tivy et al., 2011). In the Hudson Bay – Hudson Strait – Foxe Basin region, up to 70–80 % of the sea ice decline has been attributed to warmer spring and autumn surface air temperatures (SAT), respectively, wind forcing accounting for

TCD
9, 1667–1704, 2015

the balance (Hocheim and Barber, 2014). The retreating sea ice cover in Hudson Strait, immediately south of Meta Incognita Peninsula, has been accompanied by a particularly large rise in mean SAT during autumn months (SON) during or after the sea ice cover minimum, and the rate of autumn warming between 1980 and 2010 ($0.15\,^{\circ}\mathrm{C\,a^{-1}}$) is estimated to have been three times greater than the mean between 1950 and 2010 ($0.05\,^{\circ}\mathrm{C\,a^{-1}}$; Hocheim and Barber, 2014). A direct consequence of the sea ice retreat in this sector has been to increase the net solar flux received at the sea surface at an estimated average rate of $\geq 0.8\,\mathrm{W\,m^{-2}\,a^{-1}}$ over the period 1984–2006, and probably faster after the mid-1990s when sea ice decline accelerated (Matsoukas et al., 2010). The resulting positive radiative forcing is expected to be largest in mid-summer when the downwelling solar flux is at its annual maximum, and this has likely enhanced surface melt rates on glaciers of Meta Incognita Peninsula in recent decades.

The air temperature record from Iqaluit (Fig. 8a) shows that while the sum of positive degree-days (PDD) in July in this region increased by $\sim 1\,^{\circ}\mathrm{day\,a^{-1}}$ ($p < 0.05$) since the relatively cool 1960s–70s, this rate increased to $\sim 1.2\,^{\circ}\mathrm{day\,a^{-1}}$ after 1992 ($p < 0.05$). PDD recorded at Iqaluit also increased in September and October, but not noticeably in April or May. These observations suggest that increased melt rates on GIC and TNIC in recent decades may be due in part to a lengthening of the melt season in autumn, possibly linked to the later freeze-up in Hudson Strait (Hocheim and Barber, 2014). This situation would differ somewhat from that of Barnes Ice Cap (70° N), where the lengthening of the melt season was attributed to more frequent early spring thaw events (Dupont et al., 2012). With the current recession of the GIC and TNIC, we may have a clear illustration of the Arctic warming amplification effect that results from changes in surface albedo and surface heat exchange brought about by cryospheric changes over land and sea (Serreze and Barry, 2011).

TCD
9, 1667–1704, 2015

7 Conclusion

This paper highlighted historical and recent trends in area, elevation and mass changes for the two southernmost ice caps of the Canadian Arctic Archipelago, the Grinnell Ice Cap (GIC) and the Terra Nivea Ice Cap (TNIC). Our analysis is based on multiple datasets and uses an original approach where ground control points for the photogrammetric processing of old aerial photographs are derived from sub-meter resolution Pléiades stereo-images.

Results showed that the extent of the TNIC is 34 % smaller in 2014 when compared to end of the 50s' extent, while the GIC had shrunk by nearly 20 % between 1952 and 2014. Both ice caps have also experienced strong acceleration of their shrinkage rates since the beginning of the 21st century.

Historical glacier-wide mass balance has been $-0.37 \pm 0.21\,\mathrm{m\,a^{-1}}$ w.e. (1952–2014) for the GIC and slightly more negative for TNIC at $-0.47 \pm 0.16\,\mathrm{m\,a^{-1}}$ w.e. (1958/59–2014). The mass balance measured for the TNIC between 2007 and 2014 was $-1.68 \pm 0.36\,\mathrm{m\,a^{-1}}$ w.e., a rate 5.6 times as negative as the mass balance of $-0.30 \pm 0.19\,\mathrm{m\,a^{-1}}$ w.e. measured between 1958/59 and 2007. This is also twice as negative as the average mass balance obtained between 2003 and 2009 for other larger ice caps in the southern part of Baffin Island (Gardner et al., 2012).

The 2007–2014 mass balance on the TNIC is among the most negative multi-annual glacier-wide mass balances measured to date, comparable to other negative trends observed in the southern mid-latitudes (Willis et al., 2012; Berthier et al., 2009) or in South-East Alaska (Trüssel et al., 2013). This similarity underlines the strong sensitivity of maritime low-elevation ice bodies to the currently observed climate change at mid-latitudes and in polar regions (Hock et al., 2009). In the case of the southern Baffin Island, the ice cap wastage is probably due to a regional warming partly explained by a rapid decline in summer sea ice cover in this region.

Acknowledgements. Charles Papasodoro acknowledges support from the Fond Québécois de Recherche en Nature et Technologies (FQRNT) fellowship program and the Centre d'Études

TCD
9, 1667–1704, 2015

Nordiques (CEN) for an internship at LEGOS (Toulouse, France). The 2003/04 field surveys on the GIC were conducted with the able assistance of J. C. Lavergne and C. Kinnard, and logistical support from the Geological Survey of Canada, the Polar Continental Shelf Project, and the Nunavut Research Institute. D. Scott, F. Savopol, C. Armenakis and P. Sauvé (Geomatics Canada) assisted with the GPS data reduction and photogrammetric analysis. This research was support by the Natural Sciences and Engineering Research Council of Canada, by the French Space Agency (CNES) through the ISIS and TOSCA programs (Pléiades data) and by the Geological Survey of Canada (field campaign). ASTER and Landsat data were obtained free of charge thanks respectively to the GLIMS program (NSIDC) and USGS.

References

Andrews, J. T., Holdsworth, G., and Jacobs, J. D.: Glaciers of the Arctic Islands. Glaciers of Baffin Island, USGS Professional Paper 1386-J-1, J162–J198, 2002.

Astrium: Pléiades Imagery User Guide, Airbus Defence and Space, Geo-Information Services, Toulouse, 2012.

Barrand, N. E., Murray, T., James, T. D., Barr, S. L., and Mills, J. P.: Instruments and methods optimizing photogrammetric DEMs for glacier volume change assessment using laser-scanning derived ground-control points, J. Glaciol., 55, 106–116, 2009.

Beaulieu, A. and Clavet, D.: Accuracy assessment of Canadian digital elevation data using ICESat, Photogramm. Eng. Rem. S., 75, 81–86, 2009.

Berthier, E. and Toutin, T.: SPOT5-HRS digital elevation models and the monitoring of glacier elevation changes in North-West Canada and South-East Alaska, Remote Sens. Environ., 112, 2443–2454, doi:10.1016/j.rse.2007.11.004, 2008.

Berthier, E., Le Bris, R., Mabileau, L., Testut, L., and Rémy, F.: Ice wastage on the Kerguelen Islands (49S, 69E) between 1963 and 2006, J. Geophys. Res., 114, F03005, doi:10.1029/2008JF001192, 2009.

Berthier, E., Vincent, C., Magnússon, E., Gunnlaugsson, Á. Þ., Pitte, P., Le Meur, E., Masiokas, M., Ruiz, L., Pálsson, F., Belart, J. M. C., and Wagnon, P.: Glacier topography and elevation changes derived from Pléiades sub-meter stereo images, The Cryosphere, 8, 2275–2291, doi:10.5194/tc-8-2275-2014, 2014.

Blake, W.: Studies of the Grinnell Glacier, Baffin Island, Arctic, Vol. 6, 167 pp., 1953.

TCD
9, 1667–1704, 2015

Cogley, J. G., Hock, R., Rasmussen, L. A., Arendt, A. A., Bauder, A., Braithwaite, R. J., Jansson, P., Kaser, G.,Möller, M., Nicholson, L., and Zemp, M.: Glossary of Glacier Mass Balance and Related Terms, IHP-VII Technical Documents in Hydrology No. 86, IACS Contribution No. 2, UNESCO-IHP, Paris, 114 pp., 2011.

Das, I., Hock, R., Berthier, E., and Lingle, C. S.: 21st-century increase in glacier mass loss in the Wrangell Mountains, Alaska, USA, from airborne laser altimetry and satellite stereo imagery, J. Glaciol., 60, 283–293, doi:10.3189/2014JoG13J119, 2014.

Davies, B. J., Carrivick, J. L., Glasser, N. F., Hambrey, M. J., and Smellie, J. L.: Variable glacier response to atmospheric warming, northern Antarctic Peninsula, 1988–2009, The Cryosphere, 6, 1031–1048, doi:10.5194/tc-6-1031-2012, 2012.

Dowdeswell, J.: Debris transport paths and sediment flux through the Grinnell ice cap, Frobisher Bay, Baffin Island, N.W.T., Canada, unpublished MA Thesis, University of Colorado, Boulder, Colorado, 169 pp., 1982.

Dowdeswell, J.: Late quaternary chronology for Watts Bay Area, Frobisher Bay, Southern Baffin Island, N.W.T., Canada, Arctic Alpine Res., 16, 311–320, 1984.

Dupont, F., Royer, A., Langlois, A., Gressent, A., Picard, G., Fily, M., Cliche, P., and Chum, M.: Monitoring the melt season length of the Barnes Ice Cap over the 1979–2010 period using active and passive microwave remote sensing data, Hydrol. Process., 26, 2643–2652, doi:10.1002/hyp.9382, 2012.

Fox, J. A. and Nuttall, A.-M.: Photogrammetry as a research tool, Photogramm. Rec., 15, 725–737, 1997.

Fujisada, H., Bailey, G. B., Kelly, G. G., Hara, S., and Abrams, M. J.: ASTER DEM performance, IEEE T. Geosci. Remote, 43, 2707–2714, doi:10.1109/TGRS.2005.847924, 2005.

Frey, H., Paul, F., and Strozzi, T.: Compilation of a glacier inventory for the western Himalayas from satellite data: methods, challenges, and results, Remote Sens. Environ., 124, 832–843, doi:10.1016/j.rse.2012.06.020, 2012.

Gardelle, J., Berthier, E., Arnaud, Y., and Kääb, A.: Region-wide glacier mass balances over the Pamir-Karakoram-Himalaya during 1999–2011, The Cryosphere, 7, 1263–1286, doi:10.5194/tc-7-1263-2013, 2013.

Gardner, A. S., Moholdt, G., Wouters, B., Wolken, G. J., Burgess, D. O., Sharp, M. J., Cogley, J. G., Braun, C., and Labine, C.: Sharply increased mass loss from glaciers and ice caps in the Canadian Arctic Archipelago, Nature, 473, 357–60, doi:10.1038/nature10089, 2011.

TCD
9, 1667–1704, 2015

Gardner, A., Moholdt, G., Arendt, A., and Wouters, B.: Accelerated contributions of Canada's Baffin and Bylot Island glaciers to sea level rise over the past half century, The Cryosphere, 6, 1103–1125, doi:10.5194/tc-6-1103-2012, 2012.

Gardner, A. S., Moholdt, G., Cogley, J. G., Wouters, B., Arendt, A. A., Wahr, J., Berthier, E., Hock, R., Pfeffer, W. T., Kaser, G., Ligtenberg, S. R. M., Bolch, T., Sharp, M. J., Hagen, J. O., van den Broeke, M. R., and Paul, F.: A reconciled estimate of glacier contributions to sea level rise: 2003 to 2009, Science, 340, 852– 857 doi:10.1126/science.1234532, 2013.

Hannesdóttir, H., Björnsson, H., Pálsson, F., Aðalgeirsdóttir, G., and Guðmundsson, S.: Area, volume and mass changes of southeast Vatnajökull ice cap, Iceland, from the Little Ice Age maximum in the late 19th century to 2010, The Cryosphere Discuss., 8, 4681–4735, doi:10.5194/tcd-8-4681-2014, 2014.

Hock, R., de Woul, M., Radić, V., and Dyurgerov, M.: Mountain glaciers and ice caps around Antarctica make a large sea-level rise contribution, Geophys. Res. Lett., 36, 17, doi:10.1029/2008GL037020, 2009.

Hocheim, K. P. and Barber, D. G.: An update on the ice climatology of the Hudson Bay system, Arct. Antarc. Alp. Res., 46, 66–83, 2014.

Hooke, R. L., Johnson, G. W., Brugger, K. A., Hanson, B., and Holdsworth, G.: Changes in mass balance, velocity, and surface profile along a flow line on Barnes Ice Cap, 1970–1984, Can. J. Earth Sci., 24, 1550–1561, 1987.

Huss, M.: Density assumptions for converting geodetic glacier volume change to mass change, The Cryosphere, 7, 877–887, doi:10.5194/tc-7-877-2013, 2013.

Kaufman, D. S., Schneider, D. P., McKay, N. P., Ammann, C. M., Bradley, R. S., Briffa, K. R., Miller, G. H., Otto-Bliesner, B. L., Overpeck, J. T., and Vinther, B. M.: Recent warming reverses long-term arctic cooling, Science, 325, 1236–1239, doi:10.1126/science.1173983, 2009.

Koerner, R. M.: Mass balance of glaciers in the Queen Elizabeth Islands, Nunavut, Canada, Ann. Glaciol. 41, 417–423, 2005.

Matsoukas, C., Hatzianastassiou, N., Fotiadi, A., Pavlakis, K. G., and Vardavas, I.: The effect of Arctic sea-ice extent on the absorbed (net) solar flux at the surface, based on ISCCP-D2 cloud data for 19832007, Atmos. Chem. Phys., 10, 777–787, doi:10.5194/acp-10-777-2010, 2010.

Mercer, J. H.: The physiography and glaciology of southernmost of Baffin Island, unpublished PhD Thesis, McGill University, Montreal, Canada, 150 pp., 1954.

TCD
9, 1667–1704, 2015

Mercer, J. H.: The Grinnell and Terra Nivea ice caps, J. Glaciol., 19, 653–656, doi:10.3189/002214356793701910, 1956.
Muller, D. S.: Glacial geology and Quaternary history of southeast Meta Incognita Peninsula, Baffin Island, Canada, M.S. thesis, University of Colorado, Boulder, Colorado, 211 pp., 1980.
Nuth, C. and Kääb, A.: Co-registration and bias corrections of satellite elevation data sets for quantifying glacier thickness change, The Cryosphere, 5, 271–290, doi:10.5194/tc-5-271-2011, 2011.
Oerlemans, J., Anderson, B., Hubbard, A., Huybrechts, P., Johannesson, T., Knap, W. H., Schmeits, M., Stroeven, A. P., van de Wal, R. S. W., Wallinga, J., and Zuo, Z.: Modelling the response of glaciers to climate warming, Clim. Dynam., 14, 267–274, 1998.
Paul, F., Barrand, N. E., Baumann, S., Berthier, E., Bolch, T., Casey, K., Frey, H., Joshi, S. P., Konovalov, V., Bris, R. Le, Mölg, N., Nosenko, G., Nuth, C., Pope, A., Racoviteanu, A., Rastner, P., Raup, B., Scharrer, K., Steffen, S., and Winsvold, S.: On the accuracy of glacier outlines derived from remote-sensing data, Ann. Glaciol., 54, 171–182, doi:10.3189/2013AoG63A296, 2013.
PCI Geomatics: OrthoEngine User Guide, Richmond Hill, Ontario, Canada, 2013.
Pelto, M. S.: Forecasting temperate alpine glacier survival from accumulation zone observations, The Cryosphere, 4, 67–75, doi:10.5194/tc-4-67-2010, 2010.
Pfeffer, W. T., Arendt, A. A., Bliss, A., Bolch, T., Cogley, J. G., Gardner, A. S., Hagen, J.-O., Hock, R., Kaser, G., Kienholz, C., Miles, E. S., Moholdt, G., Mölg, N., Paul, F., Radić, V., Rastner, P., Raup, B. H., Rich, J., Sharp, M. J., and the Randolph consortium: The Randolph Glacier Inventory: a globally complete inventory of glaciers, J. Glaciol., 60, 537–552, doi:10.3189/2014JoG13J176, 2014.
Schutz, B. E., Zwally, H. J., Shuman, C. A., Hancock, D., and DiMarzio, J. P.: Overview of the ICESat Mission, Geophys. Res. Lett., 32, L21S01, doi:10.1029/2005GL024009, 2005.
Serreze, M. C. and Barry, R. G. Processes and impacts of Arctic amplification: a research synthesis, Global Planet. Change, 77, 85–96, 2011.
Sharp, M., Burgess, D. O., Cogley, J. G., Ecclestone, M., Labine, C., and Wolken, G. J.: Extreme melt on Canada's Arctic ice caps in the 21st century, Geophys. Res. Lett., 38, L11501, doi:10.1029/2011GL047381, 2011.
Sharp, M., Burgess, D. O., Cawkwell, F., Copland, L., Davis, J. A., Dowdeswell, E. K., Dowdeswell, J. A., Gardner, A. S., Mair, D., Wang, L., Williamson, S. N., Wolken, G. J., and Wyatt, F.: Recent glacier changes in the Canadian Arctic, in: Global Land Ice Measurements

TCD
9, 1667–1704, 2015

from Space: Satellite Multispectral Imaging of Glaciers, edited by: Kargel, J. S., Bishop, M. P., Kaab, A., Raup, B. H., and Leonard, G., Springer-Praxis, 205–228, 2014.
Sneed, W. A., Hooke, R. L., and Hamilton, G. S.: Thinning of the south dome of Barnes Ice Cap, Arctic Canada, over the past two decades, Geology, 36, 71, doi:10.1130/G24013A.1, 2008.
Soruco, A., Vincent, C., Francou, B., and Gonzalez, J. F.: Glacier decline between 1963 and 2006 in the Cordillera Real, Bolivia, Geophys. Res. Lett., 36, L03502, doi:10.1029/2008GL036238, 2009.
Tingley, M. P. and Huybers, P.: Recent temperature extremes at high northern latitudes unprecedented in the past 600 years, Nature, 496, 201–205, doi:10.1038/nature11969, 2013.
Tivy, A., Howell, E. L., Alt, B., McCourt, S., Chagnon, R.Crocker, G., Carrieres, T., and Yackel, J. J.: Trends and variability in summer sea ice cover in the Canadian Arctic based on the Canadian Ice Service Digital Archive, 1960–2008 and 1968–2008, J. Geophys. Res., 116, C03007, doi:10.1029/2009JC005855, 2011.
Trüssel, B. L., Motyka, R. J., Truffer, M., and Larsen, C. F.: Rapid thinning of lake-calving Yakutat Glacier and the collapse of the Yakutat Icefield, southeast Alaska, USA, J. Glaciol., 59, 149–161, doi:10.3189/2013J0G12J081, 2013.
Vaughan, D. G., Comiso, J. C., Allison, I., Carrasco, J., Kaser, G., Kwok, R., Mote, P., Murray, T., Paul, F., Ren, J., Rignot, E., Solomina, O., Steffen, K., and Zhang, T.: Observations: cryosphere, in: Climate Change 2013: The Physical Science Basis, Contribution of Working Group I to the Fifth Assessment Report of the Intergovernmental Panel on Climate Change, edited by: Stocker, T. F., Qin, D., Plattner, G.-K., Tignor, M., Allen, S. K., Boschung, J., Nauels, A., Xia, Y., Bex V.. and Midgley, P. M., Cambridge University Press, Cambridge, UK and New York, NY, USA, 317–382, 2013.
Wagnon, P., Vincent, C., Arnaud, Y., Berthier, E., Vuillermoz, E., Gruber, S., Ménégoz, M., Gilbert, A., Dumont, M., Shea, J. M., Stumm, D., and Pokhrel, B. K.: Seasonal and annual mass balances of Mera and Pokalde glaciers (Nepal Himalaya) since 2007, The Cryosphere, 7, 1769–1786, doi:10.5194/tc-7-1769-2013, 2013.
Way, R.: Multidecadal Recession of Grinnell and Terra Nivea Ice Caps, Baffin Island, Canada, Arctic 68, 1, doi:10.14430/arctic4461, 2015.
Weaver, R. L.: "Boas" Glacier (Baffin Island, N.W.T., Canada) mass balance for the five budget years 1969 to 1974, Arctic Alpine Res., 7, 279–284, 1975.

TCD
9, 1667–1704, 2015

Willis, M. J., Melkonian, A. K., Pritchard, M. E., and Rivera, A.: Ice loss from the Southern Patagonian Ice Field, South America, between 2000 and 2012, Geophys. Res. Lett., 39, 17, doi:10.1029/2012GL053136, 2012.

Winsvold, S. H., Andreassen, L. M., and Kienholz, C.: Glacier area and length changes in Norway from repeat inventories, The Cryosphere, 8, 1885–1903, doi:10.5194/tc-8-1885-2014, 2014.

Zdanowicz, C.: Glacier-Climate Studies on Grinnell Ice Cap – Final Research Report, Nunavut Research Institute, National Glaciology Program, Geological Survey of Canada, Ottawa, Canada, 2007.

Zemp, M., Jansson, P., Holmlund, P., Gärtner-Roer, I., Koblet, T., Thee, P., and Haeberli, W.: Reanalysis of multi-temporal aerial images of Storglaciären, Sweden (1959–99) – Part 2: Comparison of glaciological and volumetric mass balances, The Cryosphere, 4, 345–357, doi:10.5194/tc-4-345-2010, 2010.

Zemp, M., Thibert, E., Huss, M., Stumm, D., Rolstad Denby, C., Nuth, C., Nussbaumer, S. U., Moholdt, G., Mercer, A., Mayer, C., Joerg, P. C., Jansson, P., Hynek, B., Fischer, A., Escher-Vetter, H., Elvehøy, H., and Andreassen, L. M.: Reanalysing glacier mass balance measurement series, The Cryosphere, 7, 1227–1245, doi:10.5194/tc-7-1227-2013, 2013.

Zwally, H. J., Schutz, B., Abdalati, W., Abshire, J., Bentley, C., Brenner, A., Bufton, J., Dezio, J., Hancock, D., Harding, D., Herring, T., Minster, B., Quinn, K., Palm, S., Spinhirne, J., and Thomas, R.: ICESat's laser measurements of polar ice, atmosphere, ocean, and land, J. Geodyn., 34, 405–445, doi:10.1016/S0264-3707(02)00042-X 2002.

TCD
9, 1667–1704, 2015

Table 1. Elevation datasets used in this study with the acquisition date and the purpose of their use for each ice cap.

Ice cap	Elevation data set	Acquisition date	Purpose
Grinnell	Photogrammetry derived DEM	21–22 Aug 1952	Historical mass balance and d*H*
	CDED	6 Sep 1958	Absolute coregistration
	ICESat points	Whole laser periods outside glacier	Absolute coregistration
		Nov 2003, Mar 2004, Mar 2005, Nov 2005, Mar 2006, Nov 2006 and Apr 2007 (on glacier)	Recent d*H*
	In-situ GPS points	Apr 2004	Recent d*H*
	Pléiades DEM	3 Aug 2014	Historical and recent mass balances and d*H*
Terra Nivea	CDED	6 Sep 1958 (West part) and 4 Aug 1959 (East part)	Historical mass balance and d*H*, absolute coregistration
	ICESat points	Whole laser periods outside glacier	Absolute coregistration
		Apr and Nov 2007 (on glacier)	Evaluation of ASTER DEM
	ASTER DEM	3 Aug 2007	Recent mass balance and d*H*
	Pléiades DEM	14 Aug 2014 (West part) and 26 Aug 2014 (East part)	Historical and recent mass balances and d*H*

TCD
9, 1667–1704, 2015

Table 2. Historical and recent glacier-wide mass balances for both ice caps.

Ice cap	Time interval	Dataset	Data voids (%)	Mass balance (m w.e. yr^{-1})
Grinnell	1952–2014	Photogrammetric DEM and Pléiades DEM	34	−0.37 ± 0.21
Terra Nivea	1958/59–2014	CDED and Pléiades DEM	36	−0.48 ± 0.17
	1958/59–2007	CDED and ASTER DEM	21	−0.30 ± 0.19
	2007–2014	ASTER DEM and Pléiades DEM	29	−1.68 ± 0.36

TCD
9, 1667–1704, 2015

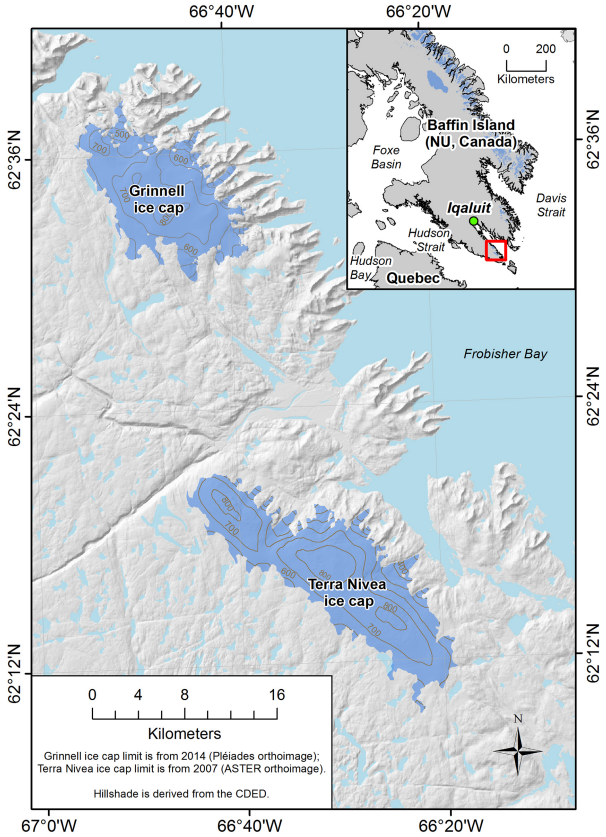

Figure 1. Study area.

TCD
9, 1667–1704, 2015

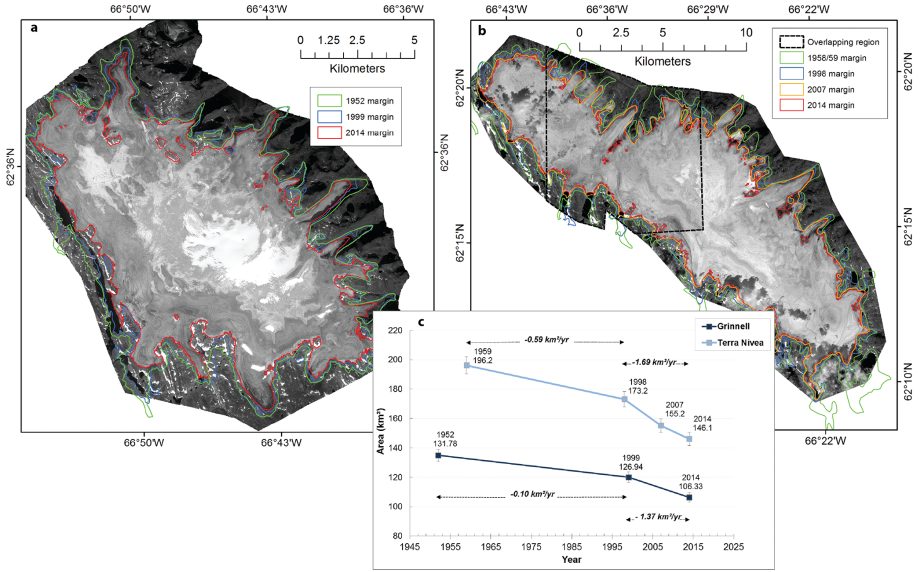

Figure 2. (a) Pléiades orthoimage of the Grinnell Ice Cap (3 August 2014) superposed by extents from 1952, 1999 and 2014 **(b)** Pléiades orthoimages of the Terra Nivea Ice Cap (14 August 2014 on the East side and 26 August 2014 on the West side) superposed by extents from 1958/59, 1998, 2007 and 2014. The overlapping area between the two orthoimages is represented by the black dashed polygon. **(c)** Historical and recent area changes for both ice caps. Error margin for each measured area is 3 %.

TCD
9, 1667–1704, 2015

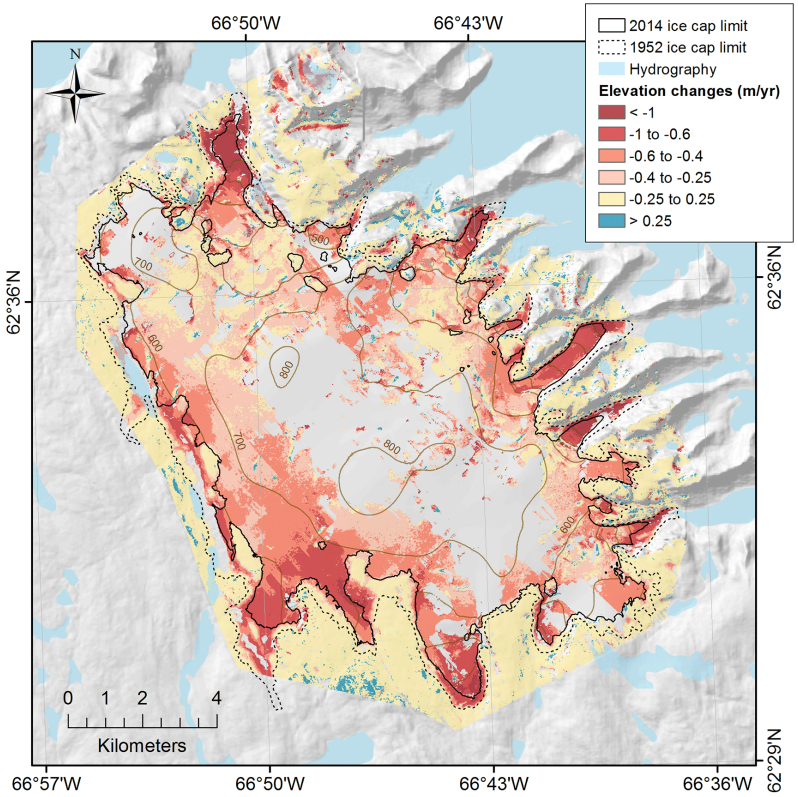

Figure 3. Elevation change rates ($m a^{-1}$) on the Grinnell Ice Cap between August 1952 (Aerial photo DEM) and August 2014 (Pléiades DEM).

TCD
9, 1667–1704, 2015

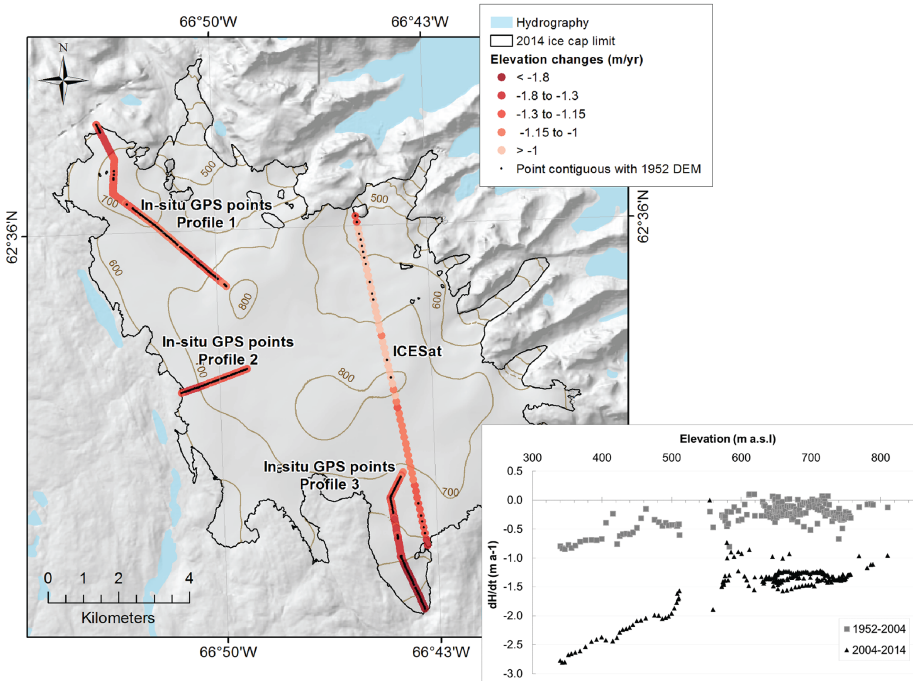

Figure 4. Elevation change rates ($m a^{-1}$) on the Grinnell Ice Cap between March–April 2004 (ICESat and In Situ GPS points) and August 2014 (Pléiades DEM). Bottom right graph shows historical (1952–2004) and recent (2004–2014) rates of elevation changes along the 203 points contiguous with the 1952 DEM (represented as black dots on the map).

TCD
9, 1667–1704, 2015

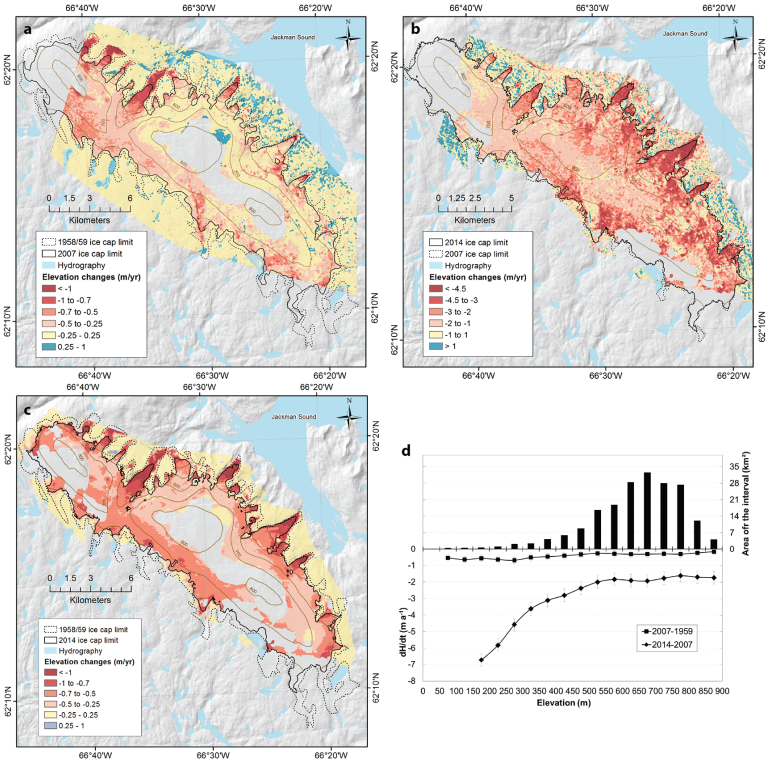

Figure 5. (a) Elevation change rates ($m a^{-1}$) on the Terra Nivea Ice Cap between 1958/59 (CDED) and 2007 (ASTER). **(b)** Elevation change rates on the Terra Nivea Ice Cap between 1958/59 (CDED) and 2014 (Pléiades DEM). **(c)** Elevation change rates on the Terra Nivea Ice Cap between 2007 (ASTER) and 2014 (Pléiades DEM). **(d)** Historical (1959–2007) and recent (2007–2014) averaged elevation changes for each 50 m elevation band on the Terra Nivea Ice Cap. The error margin is the elevation change measurement uncertainty determined in Sect. 4.4.3.

TCD
9, 1667–1704, 2015

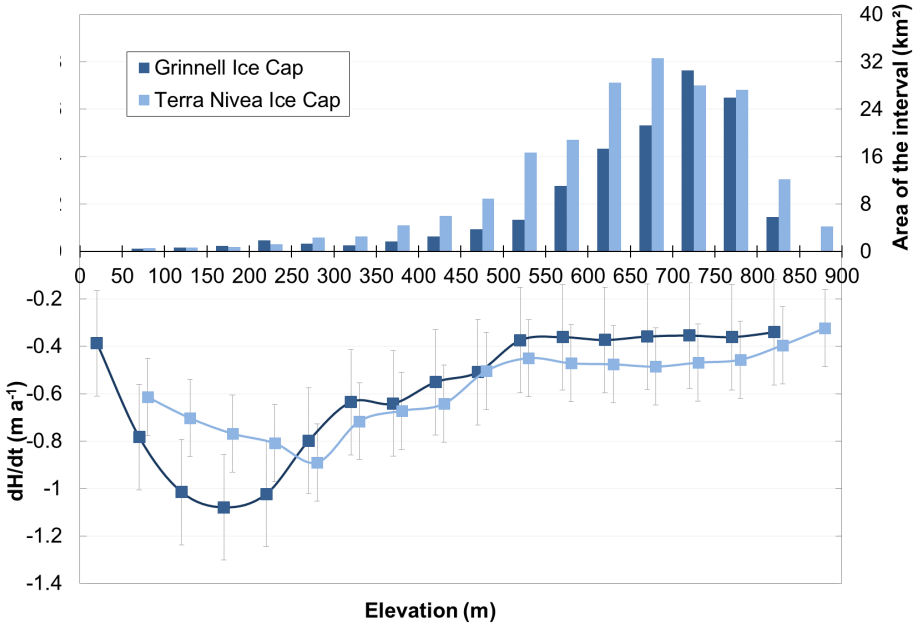

Figure 6. Historical elevation changes measured for the Grinnell (1952–2014) and the Terra Nivea (1958/59–2014) ice caps for each 50 m elevation band. The error margin is the elevation change measurement uncertainty determined in Sect. 4.4.3.

TCD
9, 1667–1704, 2015

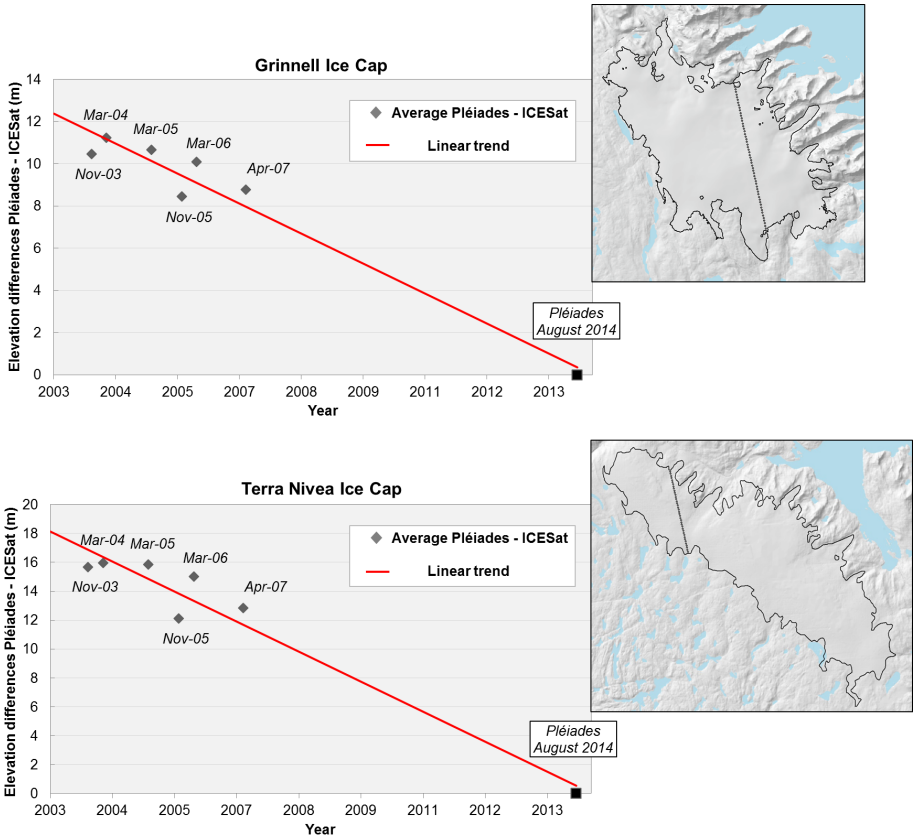

Figure 7. Recent elevation differences measured between Pléiades (2014) DEM and ICESat altimetric points. Only the complete ICESat tracks available for both ice caps were used. The trend lines indicate the mean rate of elevation changes along these two ICESat reference tracks and equals $\sim -1.1\,\mathrm{m\,yr^{-1}}$ for the Grinnell Ice Cap and $\sim -1.6\,\mathrm{m\,yr^{-1}}$ for the Terra Nivea Ice Cap. Transects location for each ice cap is shown on the inset maps (right side).

TCD
9, 1667–1704, 2015

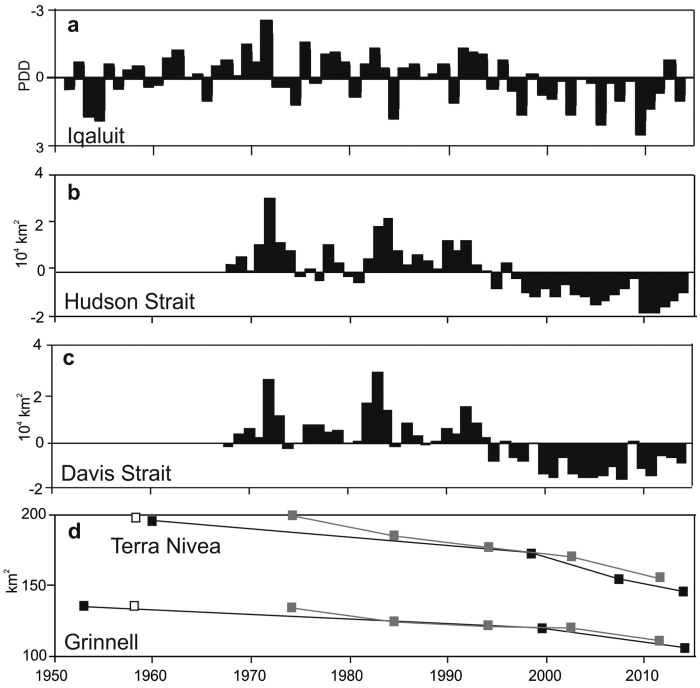

Figure 8. Annual anomalies in total positive degree-days (PDD) recorded between May and November at the Iqaluit weather station, 1952 to 2014. Vertical scale is inverted. **(b, c)** Anomalies in total sea ice covered area during the summer and autumn (25 June–19 November) over Hudson Strait and Davis Strait (respectively), 1968–2014. Data provided by the Canadian Ice Service. For region boundaries, see Tivy et al. (2011), their Fig. 4. **(d)** Black lines are changes in area extent of the GIC and the TNIC, 1952–2014, from Fig. 2 (this study). Areal extents from Way (2015) are represented by the gray lines and the white square dot is from Sharp et al. (2014).

TCD
9, 1667–1704, 2015